

Tolerance-Aware Deep Optics

Jun Dai¹ Liqun Chen^{1*} Xinge Yang² Yuyao Hu¹ Jinwei Gu³ Tianfan Xue^{4,1}

¹Shanghai AI Laboratory ²KAUST

³NVIDIA ⁴The Chinese University of Hong Kong

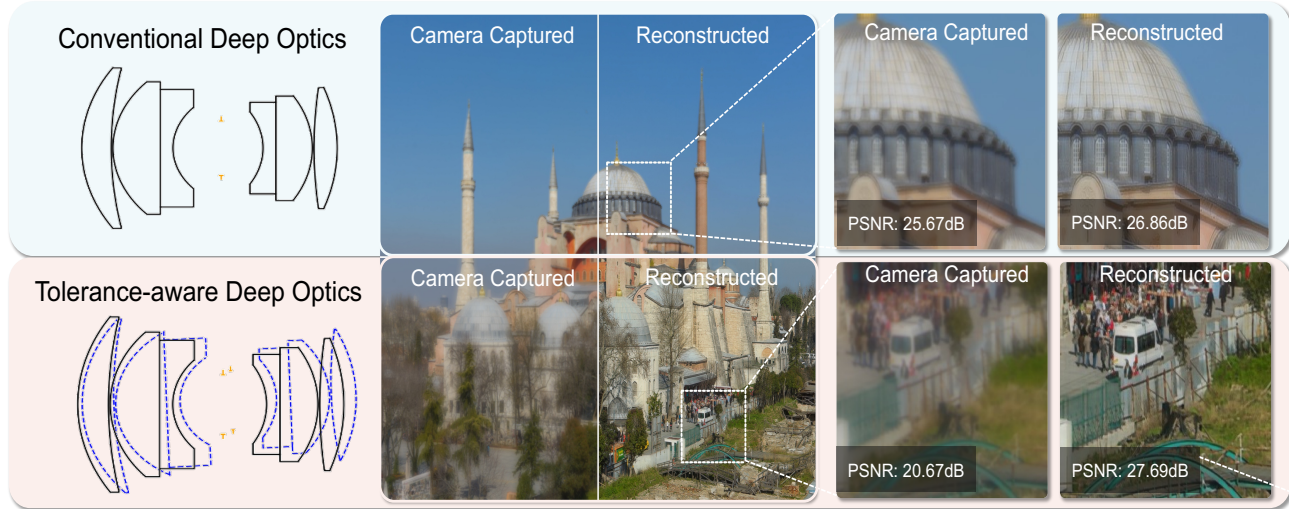


Figure 1. When subjected to random tolerances perturbations, the performance of conventional deep optics degraded severely, whereas deep optics with our tolerance-aware optimization maintained excellent computational imaging performance. *Camera Captured* and *Reconstructed*, representing the simulated camera imaging result and the reconstructed result after decoder, respectively.

Abstract

Deep optics has emerged as a promising approach by co-designing optical elements with deep learning algorithms. However, current research typically overlooks the analysis and optimization of manufacturing and assembly tolerances. This oversight creates a significant performance gap between designed and fabricated optical systems. To address this challenge, we present the first end-to-end tolerance-aware optimization framework that incorporates multiple tolerance types into the deep optics design pipeline. Our method combines physics-informed modelling with data-driven training to enhance optical design by accounting for and compensating for structural deviations in manufacturing and assembly. We validate our approach through computational imaging applications, demonstrating results in both simulations and real-world

experiments. We further examine how our proposed solution improves the robustness of optical systems and vision algorithms against tolerances through qualitative and quantitative analyses. Code and additional visual results are available at openimaginglab.github.io/LensTolerance.

1. Introduction

The concept of deep optics [30, 33, 42] has garnered significant attention for the joint optimization of optical systems and downstream vision algorithms. In a deep optics framework, the differentiable optical simulation model [31, 33, 42] and the downstream image reconstruction algorithm [19, 32] are optimized jointly in an end-to-end manner [23, 33]. This approach enables the design of novel optical systems that better support downstream tasks. End-to-end optical design [3, 29, 31, 33, 42] facilitates a tighter integration between hardware and software to achieve de-

*Corresponding author. E-mail: chenliqun@pjlab.org.cn

sign objectives, with promising example applications observed across various vision tasks, including hyperspectral imaging [22], extended depth-of-field imaging [42], high-dynamic-range (HDR) imaging [26, 32], and encoded depth estimation [17, 41]. Among existing optical systems, refractive lenses are still most widely used in practical camera platforms [10, 23, 29, 37, 45].

However, most deep optics solutions [6, 32, 41] assume perfect manufacturing and assembly processing, without any **tolerance-aware optimization**. In mass production, manufacturing and assembly errors are unavoidable and they may cause performance degradation (Sec. 3) on both the optical and algorithm sides. On the optical side, this degradation leads to a **design-to-manufacturing gap**, see Fig. 2, confining the quality of deep optics and limiting its applicability in the real world. On the algorithm side, they also hurt the performance network-based image processing, as error-free optics are assumed at network training time. Although there are several exploration from traditional tolerance optimization [13, 16, 28], to mitigate the performance gap between lens design and manufacturing, it solely considers the optical component. In an end-to-end optical design pipeline, this will disrupt the encoding and decoding relationship between the optics and algorithms (Sec. 4), compromising the integrity of the original design.

Therefore, in this work, we proposed the first deep optics learning framework that explicitly models the tolerances in manufacture and assembly. This approach allows us to sample tolerances using Monte Carlo sampling and to optimize these tolerances in an end-to-end manner, ensuring that the final design meets machining requirements while preserving the overall design performances. With this framework in place, we further define a more complete deep optics optimization flow that includes a tolerance optimization process, i.e., firstly a pre-training stage without considering tolerances, in order to obtain an initial design that meets the design objectives, and secondly, tolerance-aware optimization is used to optimize the initial design, which makes deep optics much more robust to tolerances while meeting design objectives. This more complete deep optics optimization flow greatly reduces the design-to-manufacturing gap.

Nonetheless, due to the random sampling of multiple tolerance patterns during tolerance-aware optimization, this makes it very unstable and difficult to rely exclusively on the loss functions of design objectives (Sec. 5). Therefore, to mitigate the instability and difficulty of the tolerances optimization process, we novelly design the Point Spread Function (PSF) similarity loss to enhance the robustness of the optical system to tolerances by constraining the PSF variation. In addition, we utilize Spot loss to ensure that the imaging properties of the optical system remain within reasonable range by limiting the spot size of the optical system. By combining the two proposed losses, it is possible

to complete the tolerance optimization stage stably and effectively without unduly degrading the performance of the pre-trained design.

To validate the accuracy of our tolerance modeling, we compare the ray tracing with random tolerances with Zemax [43], and the results show that our modeling accuracy is close to that of Zemax. Additionally, we compare the performance gap between deep optical designs with and without tolerance optimization under random tolerances, using computational imaging as a case study. Our results demonstrate that tolerance optimization can achieve over 2dB improvement in deblurring performance (Tab. 2). At the same time, we apply tiny perturbations to simulate tolerance perturbations during the actual images acquisition, and illustrate the effectiveness of our proposed tolerance-aware optimization by comparing the quality of the reconstructed images in the real-world experiment.

2. Related Work

Our work addresses an important problem - tolerances optimization - that has been neglected in previous deep optics. Here we review recent progress on tolerances optimization and deep optics, and highlight the main differences between existing approaches and our proposed method.

2.1. Tolerances Analysis and Optimization

Reduces the sensitivity of the optical design to tolerances and brings it in line with machining accuracy is a long standing problem in optical design. Traditional optical design typically involves a two-stage process [21], where the optical system is initially designed to fulfill the design objectives, followed by fine-tuning to align with manufacturing accuracy. The root-mean-square (RMS) or peak-to-valley (PV) values of the optical design are used to evaluate the sensitivity of optical component tolerances, as provided by conventional tolerance analysis theory [16, 24, 27]. The tolerance theory is a probabilistic statistical framework based on Monte Carlo methods [13, 28], making it suitable for the tolerance analysis of mass-produced optical components. Zemax software [43] randomly samples tolerances, analyzes the sensitivity of design parameters to these tolerances through changes in design performance, and adjusts the parameters accordingly [34].

In the context of deep optics for refractive lenses based on geometric ray tracing models, by measuring the actual Spatial Frequency response (SFR), Chen *et al.* further re-calibrated the fabricated optical design parameters that were affected by the tolerances and improved the accuracy of the imaging simulation in deep optics [8, 9]. Zhou *et al.* built on their work by adjusting the spacing between some lenses to align the simulated point spread function (PSF) with the actual measured PSF. At the same time, they employed a more powerful Mamba model [14] as the decoder, thereby

Table 1. Comparison of related work on the tolerances optimization of deep optics and computational optics, where each criterion is fully ✓, partially ✓, or not ✗ met. See text for explanations.

	Chen <i>et al.</i> [9]	Zhou <i>et al.</i> [47]	Zheng <i>et al.</i> [46]	Li <i>et al.</i> [22]	Ours
Optics Type	Lens	Lens	DOE	DOE	Lens
Optimize Parameters	✗	(✓)	✓	✓	✓
Optics & Decoder	✗	✓	✓	✓	✓
Explicit modeling	✓	✓	✗	✓	✓
Improve Robustness	✗	✗	✓	✓	✓

reducing the sensitivity of deep optics to tolerances [47]. However, the aforementioned works focus on calibrating an already machined optical system rather than end-to-end optimization of design parameters, and they do not address sensitivity to tolerances at the design stage. Closest to our work are Zheng *et al.* [46] using fabrication simulator to simulate degradation due to fabrications in computational lithography and Li *et al.* [22] in deep optics considering Diffractive Optical Elements (DOE) quantization errors due to fabrications, however, they both are not focus on lens, we list all comparisons in Tab. 1.

2.2. Deep Optics

Deep optics is an emerging field that jointly design and optimize the optical systems and vision algorithm using deep learning [39]. Sitzmann *et al.* [31] utilized this approach to design an optical element that enhances image quality. Subsequently, more works have used this method to design optics for image enhancement [4, 11, 26, 32] and depth estimation [2, 6, 15, 40]. And similar approach has been taken to design imaging lenses using differentiable ray tracing [33, 37, 42], and differentiable proxy functions [36, 41]. Tseng et al. [35] used this technique to design a metasurface lens with improved image quality. In each of these works, a differentiable model for camera’s optics is incorporated into a neural network, and the optics is designed by training the network for the specific task.

However, current deep optics models do not consider the impact of tolerances in the simulation model. This problem causes the mismatch between the designed and the fabricated lens system, which degrades reconstruction quality in physical systems. In contrast, our tolerance-aware optimization fix this mismatch by directly modeling common tolerances.

3. Methods

In this section, we introduce our tolerance-aware deep optic optimization. First, in Sec. 3.1, we introduce the definition of tolerance optimization in term of deep optics. Then, in Sec. 3.2, we explicitly model four common tolerances, decentering, tilt, curvature and central thickness errors in

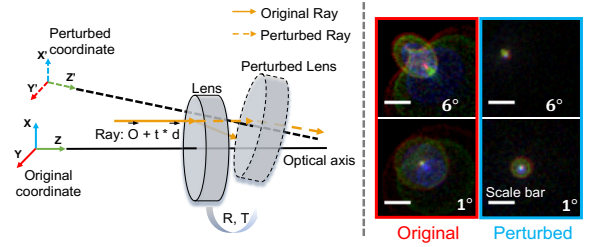


Figure 2. The tilt, decentration and central thickness tolerances can be modeled as Rotation and Translation of Lens. The spatial transformations of Lens can be equivalent to the opposite spatial transformations of ray’s coordinate. The PSFs of the lens system change drastically due to tolerances. Scale bar: 15 μ m.

the differentiable imaging process. Finally, in Sec. 3.3 and Sec. 3.4, we introduce two novel losses and present a more completed design flow for deep optics, which includes the pre-training process without tolerances and the tolerance-aware optimization that accounts for actual errors.

3.1. Tolerance Optimization for Deep Optics

In traditional optical design, tolerance optimization involves optimizing the design parameters to ensure that the degradation resulting from manufacturing or assembly errors remains within an acceptable range. Specifically, we assume the actual lens parameters θ_i at manufacturing time follows independent Gaussian distributions centered around designed parameters, $\mathcal{N}(\tilde{\theta}_i, \tilde{\sigma}_i^2)$, where $\tilde{\theta}_i$ is the design parameters without any tolerances and $\tilde{\sigma}_i^2$ is the variance of tolerance range. Then, within given ranges of tolerances t , we need to find an optimal lens parameters θ_{opt} , like curvature or spacing distance, where the imaging quality degradation is bounded as:

$$\theta_{opt}^* = \arg \max_{\theta_{opt}} \mathcal{P}(Y > Y_0 | \theta_{opt}, t), \quad (1)$$

where Y is the actual imaging quality of a lens, Y_0 is the preset performance threshold, and $\mathcal{P}(Y > Y_0)$ is the probability that the lens performance is within the designed range.

Moving to the deep optical design, the main difference is that we also need to consider the downstream image processing networks. Therefore, Eq. (1) is modified to:

$$\theta_{opt}^*, \theta_{net}^* = \arg \max_{\theta_{opt}, \theta_{net}} \mathcal{P}(Y > Y_0 | \theta_{opt}, \theta_{net}, t), \quad (2)$$

where θ_{net} is the parameters from downstream algorithms, like the parameters of neural networks. Also, Y is the performance of the downstream task, instead of imaging quality.

3.2. Modeling Tolerances in Ray Tracing

Due to the independent tolerances of each lens and the interdependence among various types of tolerances, employing

a global a priori approach to make the optical system robust against tolerances is challenging [25]. To address this, we propose explicitly modeling tolerances in every iteration of ray tracing where most of previous imaging simulation pipeline do not, allowing the optics and computational decoder to be aware of the effects of tolerances. Specifically, we use a forward ray tracing algorithm [20, 37], taking into accounts of four common lens tolerances: decentration, tilt, central thickness, and curvature errors. We perturb the original lens by these tolerances in a differentiable way and integrate them into the previous joint optimization framework.

The tolerances arising from decentration, tilt, and central thickness errors can be represented as translations and rotations of the lens surfaces, as illustrated in Fig. 2. Decentration and central thickness tolerances correspond to rigid translations of the lens in the plane perpendicular to the optical axis and along the optical axis, respectively. In contrast, the tilt tolerance can be represented as a rigid rotation of the lens, with the transformation detailed in Eq. (3). However, to simplify the verification of boundary conditions during ray tracing, we convert the rigid lens transformation into an equivalent coordinate transformation. For curvature error tolerance, a curvature offset Δc is applied in the forward ray tracing process.

In summary, to solve for the intersections of the rays with the lens during the ray tracing process, we transform the coordinates according to randomly perturbation. Then, after solving the intersection of the rays on the lens and the refraction process, we re-convert the coordinates to the original global coordinate system.

$$[\mathbf{P}', \mathbf{d}'] = \mathbf{R} \cdot [\mathbf{P} + \Delta \mathbf{T}, \mathbf{d}], \quad (3)$$

where \mathbf{P} and \mathbf{P}' are the original and perturbed ray origins, and \mathbf{d} and \mathbf{d}' are the original and perturbed ray directions; $\Delta \mathbf{T}$ is translation vector and \mathbf{R} is the rotation matrix.

3.3. Tolerance-aware Deep Optics Design

Explicitly modeling tolerances enables us to achieve tolerance-aware co-design. However, the random sampling of tolerances results in training instability, which is especially pronounced during the initial stages of deep optics optimization. Hence, we introduce a deep optics design flow that incorporates tolerance optimization and is easier to train: firstly, we employ the conventional deep optics training approach without accounting for tolerance effects, focusing solely on task performance as the design objective; secondly, once the design meets the design objectives, we conduct tolerance-aware optimization to keep its performance after fabrication.

For second tolerances optimization stage, we explicitly modeling tolerances into ray tracing process, then we use ray tracing with tolerances to implement tolerance-aware

optimization, jointly optimize both the optics and computational decoder, see in Fig. 3, to improve the robustness of deep optics design. In each iteration, we randomly sample $N = 64$ tolerances patterns and conduct forward ray tracing with sampled tolerance to render the PSF map for full field of views which contains the effects of all sampled tolerances, and use the mixed PSF map to render the sharp images by spatially-variant convolution [3, 7].

3.4. Spot Loss and PSF Similarity Loss

Since deep optics contains, optics and decoder, the difference between the number of parameters and the significance of the parameters of the two is very large, and due to the tolerance-aware optimization when randomly sampling a variety of tolerance modes, simply using the general image quality loss, such as mean-square-error loss, VGG Loss [18] and TV loss [5], the overall training difficulty is very large, see Tab. 4. In this paper, we use a basic image quality loss, $\mathcal{L}_{img} = \lambda_{vgg} \cdot \mathcal{L}_{vgg} + \lambda_{tv} \cdot \mathcal{L}_{tv} + \lambda_{mse} \cdot \mathcal{L}_{mse}$, and $\lambda_{vgg}, \lambda_{tv}$ and λ_{mse} are set in 0.001, 0.01 and 0.1.

$$\mathcal{L}_{total} = \lambda_{Spot} \cdot \mathcal{L}_{Spot} + \lambda_{PSF} \cdot \mathcal{L}_{PSF} + \mathcal{L}_{img}, \quad (4)$$

In order to improve stability the tolerances optimization for deep optics, we introduce two novel loss functions, \mathcal{L}_{Spot} and \mathcal{L}_{PSF} , in addition to basic image quality losses, \mathcal{L}_{img} . We use the spot loss, \mathcal{L}_{Spot} to constrain the spot size of lens which represent the overall imaging quality. And the PSF play the role of bridging the optics with the computational decoder, the tolerances are directly affect the PSF of lens, therefore we design \mathcal{L}_{PSF} to constrain the change of PSF under random tolerances, the two kinds of losses expressed as Eq. (5) and Eqs. (6) and (7). Noteworthy, the two new losses are directly decided by the lens, which are able to provide shortcuts for the backward gradients and improve the optimization for the lens parameters. In summary, we implement tolerance-aware optimization by loss functions, expressed Eq. (4).

$$\mathcal{L}_{Spot} = \sum_{\lambda} \sum_f \frac{\|\mathbf{P}_{\lambda,f} - \bar{\mathbf{P}}_{\lambda,f}\|_2}{N_{rays}}, \quad (5)$$

$$\mathcal{L}_{PSF} = 1.0 - \frac{\sum_f \sum_{\lambda} Sim_{\lambda,f}}{N_f N_{\lambda}}, \quad (6)$$

$$Sim_{\lambda,f} = \max(\text{Conv}(\text{PSF}_{Ideal} \text{PSF}_{Perb})), \quad (7)$$

where $\mathbf{P}_{\lambda,f}$ and $\bar{\mathbf{P}}_{\lambda,f}$ are the position of every traced ray and averaged position of given wavelength and field of view (FoV). N_{rays} , N_f and N_{λ} are the number of sampled rays, FoVs and wavelengths. $\text{Conv}(\cdot)$ represents $stride = 1$ and $padding = K/2$ convolution, and K is the resolution size of a single PSF. λ_{Spot} and λ_{PSF} are depends on lens structure.

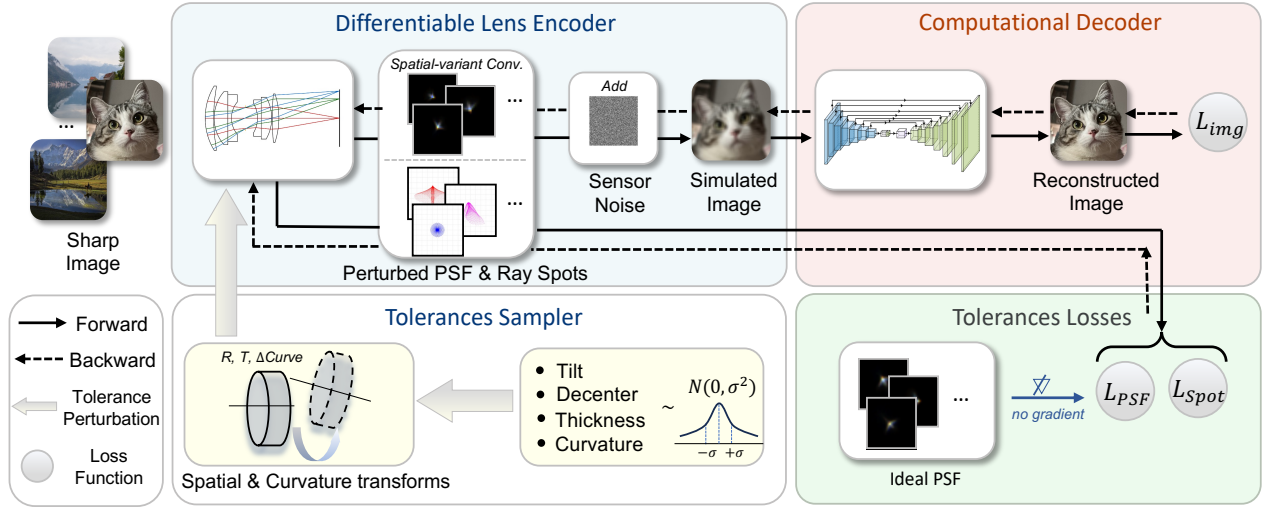


Figure 3. **Tolerance-aware optimization for deep optics.** We integrate tolerances into differentiable ray tracing. Every kind of tolerances are randomly sampled from its distribution $\mathcal{N}(0, \sigma_i^2)$, use ray tracing with tolerances to render perturbed spatially-variant PSF maps and simulated the imaging results by spatially-variant convolution, then noise is added to simulate sensor-captured images. These images are then passed to a computational decoder for reconstruction. During forward simulation, we track gradients of optical parameters, We can subsequently back-propagate the errors from either the reconstruction images quality and tolerance loss terms. The framework jointly optimizes the optics and the computational decoder in a tolerance-aware manner.

4. Experiments

We conduct our experiments based on the open-source differentiable ray tracer DeepLens [37, 42]. We firstly compare the ray tracing results of our framework with Zemax [43] to demonstrate the accuracy of imaging simulation with tolerances in Sec. 4.1. And in Sec. 4.2 and Sec. 4.3, we implement computational imaging task to validate the effectiveness of the tolerance-aware optimization in simulation and real-world levels. Finally, in Sec. 4.4, we analyze how tolerance-aware optimization improve deep optics robustness to tolerances from both quantitative and qualitative perspectives.

4.1. Tolerance-aware Differentiable Ray-tracing

Using the method described in Sec. 3.2, we capture the deviations caused by random tolerance perturbations during the ray tracing process. This approach preserves the differentiability of the conventional deep optics pipeline, enabling accurate imaging simulations in the presence of tolerances. We demonstrate that the ray tracing with tolerances is quite accurate, compared the ray tracing results with Zemax [43]. We choose a classical optical design, Cooke Triplet, and randomly sample tolerances pattern to perturb the lens system.

We visualize the ray tracing results come from Zemax [43] and ours, as shown in Fig. 4, and also calculate the root-mean-square spot sizes. The spot sizes and the overall rays distribution are nearly identical across each field-of-views,

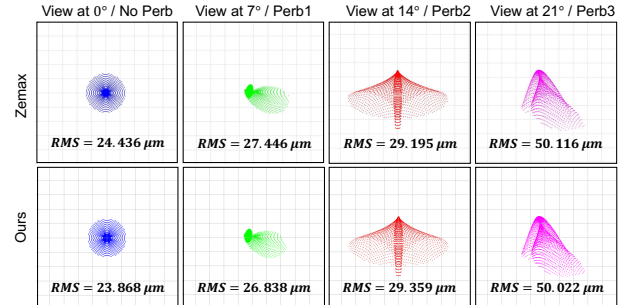


Figure 4. Spot diagrams and RMS spot sizes produced by our framework with and without perturbations are highly resemble those by Zemax, the tested lens is Cooke Triplet and for visualization, the scale bars are different.

with errors $< 1\mu m$, which shown that our ray tracing with tolerances is extremely accurate, thus it means that we are able to simulate the imaging process when lens encounter tolerances and remain differentiable manner of deep optics pipeline.

4.2. Tolerance-aware Evaluation by Simulation

To demonstrate that our tolerance-aware optimization provides better robustness and less degradation when subjected to tolerances, we compare the average deblurring results of the tolerance-aware deep optics design and the non-tolerance-aware counterpart under random tolerances, tested on the DIV2K dataset [1], shown in Tab. 2. The design with tolerance-aware optimization, has better average

Table 2. Up: the numerical results of multiple (100 times) random sampled tolerances pattern test on DIV2K test datasets for without, with our tolerance-aware optimization and conduct tolerance optimization by Zemax [43]. Bottom: the manufacturing yield result based on 100 times results, e.g., > 90% means that have 90% confidence to get PSNR > 26.26dB for Lens1 after fabrications.

Optics	Test with tolerances				Optics	Test with tolerances					
	Spot _↓ (μm)	PSNR _↑ [12]	SSIM _↑ [38]	LPIPS _↓ [44]		Spot _↓ (μm)	PSNR _↑	SSIM _↑	LPIPS _↓		
Lens1	w/ TOLR	16.2	29.61	0.847	0.293	w/ TOLR	38.7	28.08	0.850	0.225	
	w/o TOLR	7.3	29.25	0.828	0.268	Lens2	w/ TOLR	14.2	25.75	0.735	0.334
	Zemax	6.2	29.14	0.824	0.270		Zemax	9.7	23.58	0.779	0.248
Manufacturing Yield (PSNR)											
Lens1	> 90%	> 70%	> 50%	> 10%			> 90%	> 70%	> 50%	> 10%	
	w/ TOLR	26.26	29.18	30.47	31.19	Lens2	w/ TOLR	24.84	27.03	28.55	30.13
	w/o TOLR	24.30	26.68	29.15	33.82		w/o TOLR	21.94	24.26	26.40	30.66
	Zemax	24.13	26.55	29.08	34.11		Zemax	20.95	22.25	23.26	26.48

deblurring performances when encounter tolerances, the average PSNR improved by more than 2dB.

We also compare our tolerance-aware design with tolerance optimized by Zemax [43] which use Zemax to implement tolerances optimization merely by optical metrics alone, it shown that optimized by Zemax may incur the mismatch problem between optical and decoder part, thus lead the deblurring performance drop down severely (see Lens2 in Tab. 2).

At last, we analyze the manufacturing yields of the three design approaches based on our test results, which showed that deep optics demonstrated higher manufacturing yields after tolerance-aware optimization, shown in Tab. 2.

4.3. Real-world Experiment

To demonstrate the applicability of our method to real-world systems, we employ actual optical systems to acquire images and perform computational imaging. This shows that the tolerance-aware deep optics produces superior deblurring results in real-world which exist random tolerances. Specifically, we use an off-the-shelf industrial camera lens design to train and optimize the decoder both with and without tolerances optimization. We simulate tolerances by introducing slight perturbations during image acquisition and compare the quality of reconstructed images before and after optimizing the decoder for tolerances. This comparison highlights the enhanced resistance to potential tolerances provided by the optimized decoder, see Fig. 6.

4.4. Robustness Improvement of Deep Optics

The tolerance-aware optimization significantly enhances the robustness of the deep optics against potential tolerances. However, what specific factors contribute to this increased tolerances resistance following the optimization?

To understand the underlying reasons, we qualitatively analyze changes in both the optics and decoder components after tolerance optimization. For the lens, we validate its tolerance robustness by comparing the degree of PSF vari-

ation in designs with and without tolerances optimization when affected by tolerances. By assessing how the PSFs change when subjected to random tolerances, using cosine similarity to quantify the similarity between the perturbed PSF and the ideal PSF, as shown in Fig. 7. It is evident that the lens optimized with tolerance-aware can maintain the PSF within a relatively similar range, even when subject to tolerance disturbances. This greatly reduces the difficulty for the computational decoder to handle the changes of encoded patterns with tolerances.

Regarding the decoder, given the increased robustness of the lens post-optimization, we expand the range of tolerances to compare the decoder's ability to handle tolerance before and after tolerance optimization under equivalent conditions, as shown in Fig. 8. The results demonstrate that with tolerance-aware optimization, the decoder become robust to potential tolerances. After tolerance-aware optimization, the lens can maintain PSF stability, and the decoder shows greater adaptability to tolerances. This significantly enhances the resistance of deep optics to manufacturing and assembly tolerances.

5. Discussion and Ablation Study

We provide an in-depth analysis of our optimization setting, the impact of different loss functions, and the number of tolerances sampled during optimization. This analysis aims to offer more guidance for future work.

5.1. Partially Tolerance Optimization

In deep optics, the optimization of optical and decoder parameters may vary [36]. Tolerance-aware optimization adds further complexity by introducing random perturbations in each forward pass. To delve into the distinctions between these components, we selectively control the optimization: (a) optimizing the optics, and (b) only the computational decoder. Through experiments, we find that the deep optics achieves improvement of robustness only when the optics



Figure 5. Deblurring results comparison of deep optics with and without tolerance-aware optimization under tolerances perturbations. The deep optics with tolerances optimization maintain better deblurring performances than its counterpart.

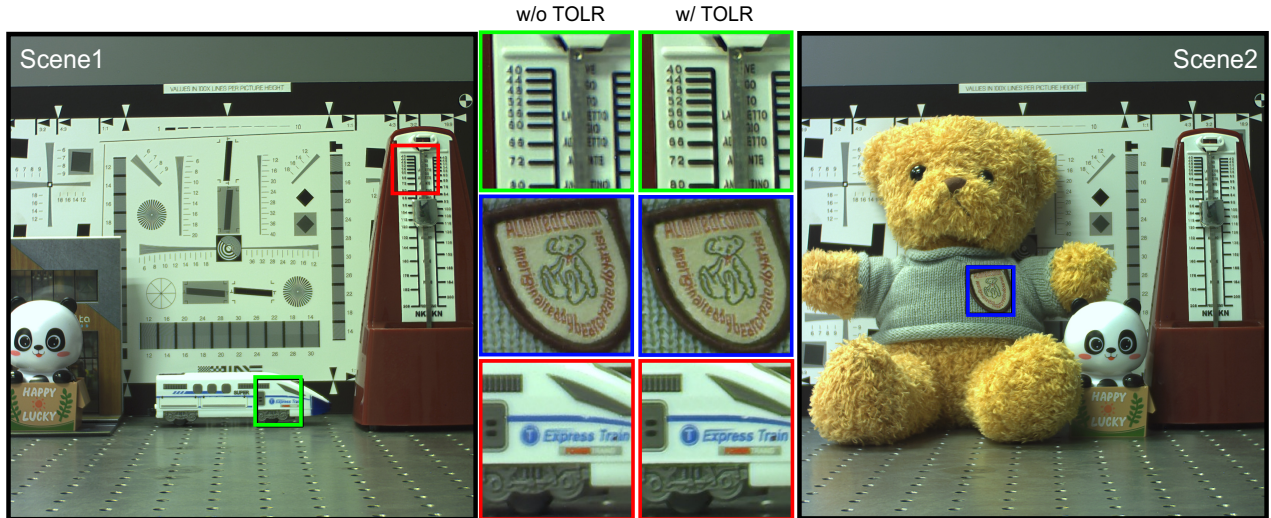


Figure 6. Physical experiment results demonstrating the robustness of our tolerance-aware deep optics. Despite random tolerance perturbations, our method maintains high deblurring performance in two distinct scenes. In contrast, the deep optics baseline without tolerance-aware optimization suffers from significant performance degradation.

and decoder are jointly optimized simultaneously, shown in Tab. 3. Optimizing only the decoder can enhance the decoder’s tolerance-aware ability, but still fails to fully address the impact of random tolerances. Additionally, when optimizing the optics alone, the global influence of optical parameters on the subsequent decoder, along with the lim-

ited number of optical parameters, makes the optimization challenging and risks compromising the results of the initial pre-training stage. Only through the joint optimization of the optical system and decoder can we achieve a more stable optical system with enhanced pairing capability from the decoder, significantly improving the robustness of deep

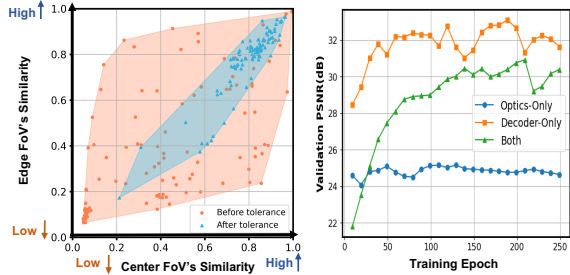


Figure 7. Qualitative analysis results for the optics (random test 50 times) and the validation PSNR values during training (test without tolerances).

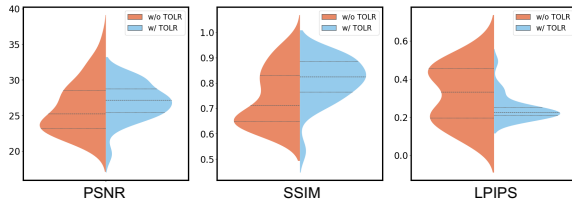


Figure 8. Qualitative analysis results for the decoder's robustness improvements. The fitted probability density distributions of 50 times of random tolerance tests of PSNR, SSIM and LPIPS. With and without tolerance optimization and for deep optics with tolerance-aware optimization is tested under larger range of tolerances.

Table 3. *Optics/Decoder-only* means that only optimize the optics/decoder part of parameters during tolerance optimization and *Both* means optimized both parts. The results are average of 100 times of random sampled tolerances experiments (excluding Spot Size).

	Optics-only	Decoder-only	Both
PSNR↑	22.06	25.94	28.08
SSIM↑	0.376	0.734	0.845
LPIPS↓	0.664	0.379	0.225
Spot Size (μm)↓	34.2	14.2	38.7

optics against potential tolerances.

5.2. Analysis of Loss Function Impact

To analyze the impact of the two loss functions, we conduct ablation studies on Spot loss and PSF loss. The experimental results are shown in Tab. 4. The results demonstrate that the proposed Spot loss and PSF loss significantly improve the performance. It is worth noting that Spot loss and PSF similarity loss can only be used together to maximize the performance of tolerance-aware optimization. The two losses play different roles respectively, the Spot loss is helpful to ensure that the overall imaging quality of the optics is not seriously degraded during the tolerance optimization, while the PSF loss is able to significantly improve the ro-

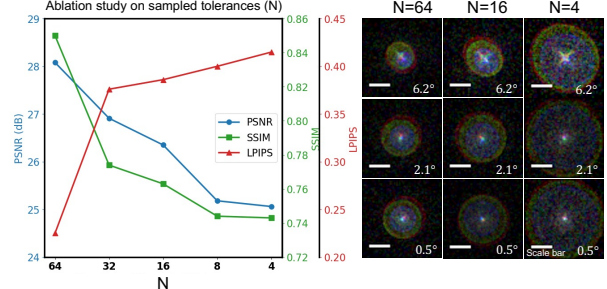


Figure 9. Ablation study on the number of sampled tolerances pattern in every iteration. Average PSNR, SSIM, and LPIPS of 100 times random tolerances test for different sampling numbers are shown, along with the PSFs comparison. Scale bar: 15 μm .

Table 4. Ablation study on Spot loss and PSF loss, each incorporating basic image quality loss. The results represent the averages from 100 random sampling tolerance experiments (excluding Spot Size).

	-	$\mathcal{L}_{\text{Spot}}$	\mathcal{L}_{PSF}	$\mathcal{L}_{\text{Spot}} \& \mathcal{L}_{\text{PSF}}$
PSNR↑	24.83	26.63	20.49	28.08
SSIM↑	0.738	0.782	0.601	0.850
LPIPS↓	0.378	0.248	0.529	0.225
Spot Size (μm)↓	52.6	12.9	637.9	38.7

bustness of the optics to random tolerances on this basis. Without the constraint of Spot loss, PSF loss can lead to significant degradation in the imaging performance of the optical system, thereby impacting overall tolerance optimization. As shown in Tab. 4, the spot size is extremely large, indicating very low imaging quality.

5.3. Number of Sampled Tolerance Patterns

In the tolerance-aware optimization process, the number of sampled tolerance patterns is a critical hyperparameter that significantly impacts the performance. If the number is too low, the optimization may stuck in local optima. However, increasing the sampled number leads to a higher consumption of GPU memory. Therefore, selecting an appropriate sample number is of great importance to balance the trade-off between optimization effectiveness and memory usage. Therefore, we employ different number of sampled tolerance pattern and conduct quantitative analysis to determine a reasonable lower limit, see in Fig. 9. This experiment significantly streamlines subsequent research efforts.

6. Conclusion

In this paper, we present a novel end-to-end approach to bridge the gap between design and manufacturing in deep optics. By integrating tolerance modeling into the ray tracing process, we achieve effective tolerance-aware optimization, resulting in a more robust and complete deep optics design flow. Our analysis shows significant improvements in

robustness, demonstrated through simulations and physical experiments. We believe this work effectively closes the divide between design and manufacturing, unlocking the potential of deep optics for mass production.

References

- [1] Eirikur Agustsson and Radu Timofte. Ntire 2017 challenge on single image super-resolution: Dataset and study. In *Proceedings of the IEEE conference on computer vision and pattern recognition workshops*, pages 126–135, 2017. [5](#), [1](#)
- [2] Seung-Hwan Baek, Hayato Ikoma, Daniel S Jeon, Yuqi Li, Wolfgang Heidrich, Gordon Wetzstein, and Min H Kim. Single-shot hyperspectral-depth imaging with learned diffractive optics. In *Proceedings of the IEEE/CVF International Conference on Computer Vision*, pages 2651–2660, 2021. [3](#)
- [3] Xin Cai, Zhiyuan You, Hailong Zhang, Wentao Liu, Jinwei Gu, and Tianfan Xue. Phocolens: Photorealistic and consistent reconstruction in lensless imaging. *arXiv preprint arXiv:2409.17996*, 2024. [1](#), [4](#)
- [4] Praneeth Chakravarthula, Jipeng Sun, Xiao Li, Chenyang Lei, Gene Chou, Mario Bijelic, Johannes Froesch, Arka Majumdar, and Felix Heide. Thin on-sensor nanophotonic array cameras. *ACM Transactions on Graphics (TOG)*, 42(6):1–18, 2023. [3](#)
- [5] Antonin Chambolle, Vicent Caselles, Daniel Cremers, Matteo Novaga, Thomas Pock, et al. An introduction to total variation for image analysis. *Theoretical foundations and numerical methods for sparse recovery*, 9(263–340):227, 2010. [4](#)
- [6] Julie Chang and Gordon Wetzstein. Deep optics for monocular depth estimation and 3d object detection. In *Proceedings of the IEEE/CVF International Conference on Computer Vision*, pages 10193–10202, 2019. [2](#), [3](#)
- [7] Shiqi Chen, Huajun Feng, Keming Gao, Zhihai Xu, and Yuetong Chen. Extreme-quality computational imaging via degradation framework. In *Proceedings of the IEEE/CVF International Conference on Computer Vision*, pages 2632–2641, 2021. [4](#)
- [8] Shiqi Chen, Huajun Feng, Dexin Pan, Zhihai Xu, Qi Li, and Yuetong Chen. Optical aberrations correction in postprocessing using imaging simulation. *ACM Transactions on Graphics (TOG)*, 40(5):1–15, 2021. [2](#)
- [9] Shiqi Chen, Ting Lin, Huajun Feng, Zhihai Xu, Qi Li, and Yuetong Chen. Computational optics for mobile terminals in mass production. *IEEE Transactions on Pattern Analysis and Machine Intelligence*, 45(4):4245–4259, 2022. [2](#), [3](#)
- [10] Geoffroi Côté, Fahim Mannan, Simon Thibault, Jean-François Lalonde, and Felix Heide. The differentiable lens: Compound lens search over glass surfaces and materials for object detection. In *Proceedings of the IEEE/CVF Conference on Computer Vision and Pattern Recognition*, pages 20803–20812, 2023. [2](#)
- [11] Xiong Dun, Hayato Ikoma, Gordon Wetzstein, Zhanshan Wang, Xinbin Cheng, and Yifan Peng. Learned rotationally symmetric diffractive achromat for full-spectrum computational imaging. *Optica*, 7(8):913–922, 2020. [3](#)
- [12] Fernando A Fardo, Victor H Conforto, Francisco C de Oliveira, and Paulo S Rodrigues. A formal evaluation of psnr as quality measurement parameter for image segmentation algorithms. *arXiv preprint arXiv:1605.07116*, 2016. [6](#)
- [13] David P Forse. Statistical tolerancing for optics. In *Specification, Production, and Testing of Optical Components and Systems*, pages 18–27. SPIE, 1996. [2](#)
- [14] Albert Gu and Tri Dao. Mamba: Linear-time sequence modeling with selective state spaces. *arXiv preprint arXiv:2312.00752*, 2023. [2](#)
- [15] Harel Haim, Shay Elmalem, Raja Giryes, Alex M Bronstein, and Emanuel Marom. Depth estimation from a single image using deep learned phase coded mask. *IEEE Transactions on Computational Imaging*, 4(3):298–310, 2018. [3](#)
- [16] Xinda Hu and Hong Hua. Design and tolerance of a free-form optical system for an optical see-through multi-focal-plane display. *Applied Optics*, 54(33):9990–9999, 2015. [2](#)
- [17] Hayato Ikoma, Cindy M Nguyen, Christopher A Metzler, Yifan Peng, and Gordon Wetzstein. Depth from defocus with learned optics for imaging and occlusion-aware depth estimation. In *2021 IEEE International Conference on Computational Photography (ICCP)*, pages 1–12. IEEE, 2021. [2](#)
- [18] Justin Johnson, Alexandre Alahi, and Li Fei-Fei. Perceptual losses for real-time style transfer and super-resolution. In *Computer Vision–ECCV 2016: 14th European Conference, Amsterdam, The Netherlands, October 11–14, 2016, Proceedings, Part II 14*, pages 694–711. Springer, 2016. [4](#)
- [19] Jeremy Klotz and Shree K Nayar. Minimalist vision with freeform pixels. In *European Conference on Computer Vision*, pages 329–346. Springer, 2025. [1](#)
- [20] Craig Kolb, Don Mitchell, and Pat Hanrahan. A realistic camera model for computer graphics. In *Proceedings of the 22nd annual conference on Computer graphics and interactive techniques*, pages 317–324, 1995. [4](#)
- [21] Milton Laikin. *Lens design*. Crc Press, 2018. [2](#)
- [22] Lingen Li, Lizhi Wang, Weitao Song, Lei Zhang, Zhiwei Xiong, and Hua Huang. Quantization-aware deep optics for diffractive snapshot hyperspectral imaging. In *Proceedings of the IEEE/CVF Conference on Computer Vision and Pattern Recognition*, pages 19780–19789, 2022. [2](#), [3](#)
- [23] Zongling Li, Qingyu Hou, Zhipeng Wang, Fanjiao Tan, Jin Liu, and Wei Zhang. End-to-end learned single lens design using fast differentiable ray tracing. *Optics Letters*, 46(21):5453–5456, 2021. [1](#), [2](#)
- [24] Milan Maksimovic. Optical design and tolerancing of freeform surfaces using anisotropic radial basis functions. *Optical Engineering*, 55(7):071203–071203, 2016. [2](#)
- [25] James P McGuire. Designing easily manufactured lenses using a global method. In *International Optical Design Conference*, page TuA6. Optica Publishing Group, 2006. [4](#)
- [26] Christopher A Metzler, Hayato Ikoma, Yifan Peng, and Gordon Wetzstein. Deep optics for single-shot high-dynamic-range imaging. In *Proceedings of the IEEE/CVF Conference on Computer Vision and Pattern Recognition*, pages 1375–1385, 2020. [2](#), [3](#)

- [27] Junhao Ni, Tong Yang, Yue Liu, Dewen Cheng, and Yongtian Wang. Description and tolerance analysis of freeform surface figure error using specific-probability-distributed gaussian radial basis functions. *Optics express*, 27(22):31820–31839, 2019. 2
- [28] Don Oinen. A new approach to the simulation of optical manufacturing processes. In *Optical Fabrication and Testing*, page JWC3. Optica Publishing Group, 1990. 2
- [29] Yifan Peng, Qilin Sun, Xiong Dun, Gordon Wetzstein, Wolfgang Heidrich, and Felix Heide. Learned large field-of-view imaging with thin-plate optics. *ACM Trans. Graph.*, 38(6):219–1, 2019. 1, 2
- [30] Vincent Sitzmann, Steven Diamond, Yifan Peng, Xiong Dun, Stephen Boyd, Wolfgang Heidrich, Felix Heide, and Gordon Wetzstein. End-to-end optimization of optics and image processing for achromatic extended depth of field and super-resolution imaging. *ACM Transactions on Graphics*, 37(4):1–13, 2018. 1
- [31] Vincent Sitzmann, Steven Diamond, Yifan Peng, Xiong Dun, Stephen Boyd, Wolfgang Heidrich, Felix Heide, and Gordon Wetzstein. End-to-end optimization of optics and image processing for achromatic extended depth of field and super-resolution imaging. *ACM Transactions on Graphics (TOG)*, 37(4):1–13, 2018. 1, 3
- [32] Qilin Sun, Ethan Tseng, Qiang Fu, Wolfgang Heidrich, and Felix Heide. Learning rank-1 diffractive optics for single-shot high dynamic range imaging. In *Proceedings of the IEEE/CVF conference on computer vision and pattern recognition*, pages 1386–1396, 2020. 1, 2, 3
- [33] Qilin Sun, Congli Wang, Fu Qiang, Dun Xiong, and Heidrich Wolfgang. End-to-end complex lens design with differentiable ray tracing. *ACM Trans. Graph.*, 40(4):1–13, 2021. 1, 3
- [34] Synopsys. Optical design tolerancing, 2015. Available: <https://www.synopsys.com/content/dam/synopsys/optical-solutions/documents/whitepapers/optical-design-tolerancing.pdf>. 2
- [35] Ethan Tseng, Shane Colburn, James Whitehead, Luocheng Huang, Seung-Hwan Baek, Arka Majumdar, and Felix Heide. Neural nano-optics for high-quality thin lens imaging. *Nature communications*, 12(1):6493, 2021. 3
- [36] Ethan Tseng, Ali Mosleh, Fahim Mannan, Karl St-Arnaud, Avinash Sharma, Yifan Peng, Alexander Braun, Derek Nowrouzezahrai, Jean-Francois Lalonde, and Felix Heide. Differentiable compound optics and processing pipeline optimization for end-to-end camera design. *ACM Transactions on Graphics (TOG)*, 40(2):1–19, 2021. 3, 6
- [37] Congli Wang, Ni Chen, and Wolfgang Heidrich. do: A differentiable engine for deep lens design of computational imaging systems. *IEEE Transactions on Computational Imaging*, 8:905–916, 2022. 2, 3, 4, 5
- [38] Zhou Wang, Alan C Bovik, Hamid R Sheikh, and Eero P Simoncelli. Image quality assessment: from error visibility to structural similarity. *IEEE transactions on image processing*, 13(4):600–612, 2004. 6
- [39] Gordon Wetzstein, Aydogan Ozcan, Sylvain Gigan, Shanhui Fan, Dirk Englund, Marin Soljačić, Cornelia Denz, David AB Miller, and Demetri Psaltis. Inference in artificial intelligence with deep optics and photonics. *Nature*, 588(7836):39–47, 2020. 3
- [40] Yicheng Wu, Vivek Boominathan, Huaijin Chen, Aswin Sankaranarayanan, and Ashok Veeraraghavan. Phase-cam3d—learning phase masks for passive single view depth estimation. In *2019 IEEE International Conference on Computational Photography (ICCP)*, pages 1–12. IEEE, 2019. 3
- [41] Xinge Yang, Qiang Fu, Mohamed Elhoseiny, and Wolfgang Heidrich. Aberration-aware depth-from-focus. *IEEE Transactions on Pattern Analysis and Machine Intelligence*, 2023. 2, 3
- [42] Xinge Yang, Qiang Fu, and Wolfgang Heidrich. Curriculum learning for ab initio deep learned refractive optics. *Nature communications*, 15(1):6572, 2024. 1, 2, 3, 5
- [43] Zemax. Opticstudio, 2013. Available: <https://www.zemax.com/>. 2, 5, 6
- [44] Richard Zhang, Phillip Isola, Alexei A Efros, Eli Shechtman, and Oliver Wang. The unreasonable effectiveness of deep features as a perceptual metric. In *Proceedings of the IEEE conference on computer vision and pattern recognition*, pages 586–595, 2018. 6
- [45] Yuanlong Zhang, Xiaofei Song, Jiachen Xie, Jing Hu, Jiawei Chen, Xiang Li, Haiyu Zhang, Qiqun Zhou, Lekang Yuan, Chui Kong, et al. Large depth-of-field ultra-compact microscope by progressive optimization and deep learning. *Nature Communications*, 14(1):4118, 2023. 2
- [46] Cheng Zheng, Guangyuan Zhao, and Peter TC So. Neural lithography: Close the design-to-manufacturing gap in computational optics with a’real2sim’learned photolithography simulator. *arXiv preprint arXiv:2309.17343*, 2023. 3
- [47] Jingwen Zhou, Bingkun Chen, Jiapu Yan, Zheng Ren, Wenguang Zhang, Huajun Feng, Yuetong Chen, and Meijuan Bian. Optical degradation correction of manufacturing-perturbed glass-plastic hybrid lens systems via a joint hardware-software optimization framework. *Optics Express*, 32(15):25866–25882, 2024. 3

Tolerance-Aware Deep Optics

Supplementary Material

A. Tolerances sampler

In this section, we present more implementation details of our tolerance sampler and its integration into the ray tracing. We model four common kinds of tolerances: decentration, tilt, central thickness, and curvature errors, and the specific tolerance ranges we used see Tab. A1. Considering the perturbations arising from tolerances in the design parameters, we can express the parameters as follows:

$$\theta_{real} = \theta_{ideal} + \theta_{\Delta}, \quad (\text{A1})$$

where θ_{ideal} is the design parameters from pretrained without considering tolerances, θ_{Δ} is the perturbations come from random tolerances, θ_{real} is the optics parameters after fabrication.

We firstly random sample tolerances from given ranges, thus, θ_{Δ} obeys the normal distribution, $\theta_{\Delta} \sim \mathcal{N}(0, \frac{max^2}{9})$, so that the range of tolerances is approximately 3 times the standard deviation of the normal distribution, *e.g.*, for decentration, $max = 0.04mm$, and we clamp the tolerances range if sampled tolerance values exceed the max . Secondly, for each individual lens (or double glued structure) in the lens system, we independently sample four tolerances.

Given that we are conducting ray tracing on a surface-by-surface basis, we convert the sampled per-lens tolerances into the necessary spatial transformations and curvature offsets for each surface. First, we categorize the tolerances into two types: spatial transformations, which include decentration, tilt, and central thickness error, and curvature errors, which can be implemented as offsets in the ray tracing process. Notably, both decentration and central thickness errors are consolidated into a single translation of the lens surfaces, expressed as translation vector $\mathbf{T} = [\Delta X, \Delta Y, \Delta Z]^T$. While tilt is represented as a rotation of the lens surfaces, expressed as Rotation matrix, $\mathbf{R} = \mathbf{R}_z(\gamma) \cdot \mathbf{R}_y(\beta) \cdot \mathbf{R}_x(\alpha)$, more specific:

$$\mathbf{R}_x(\alpha) = \begin{bmatrix} 1 & 0 & 0 \\ 0 & \cos \alpha & \sin \alpha \\ 0 & \sin \alpha & \cos \alpha \end{bmatrix}, \quad (\text{A2})$$

$$\mathbf{R}_y(\beta) = \begin{bmatrix} \cos \beta & 0 & \sin \beta \\ 0 & 1 & 0 \\ -\sin \beta & 0 & \cos \beta \end{bmatrix}, \quad (\text{A3})$$

$$\mathbf{R}_z(\gamma) = \begin{bmatrix} \cos \gamma & -\sin \gamma & 0 \\ \sin \gamma & \cos \gamma & 0 \\ 0 & 0 & 1 \end{bmatrix}. \quad (\text{A4})$$

where α, β, γ are sampled tilt degrees from normal distribution, around three axes.

Table A1. Specific tolerance ranges use in our paper. Decentration and central thickness error tolerances are in *millimeters*, curvature error is in *percentage* and tilt is in *degree*.

	TOLR Range
Decentration	(−0.04, 0.04)
Tilt	(−0.05, 0.05)
Central thickness error	(−0.04, 0.04)
Curvature error	(−0.3%, +0.3%)

As we convert the surface transformations into equivalent coordinate system transformations, we need to invert the signs of the formulas above. In the ray tracing process, we first apply the coordinate system transformations in the order of translation followed by rotation. We then calculate the intersection point between the ray and the surface, incorporating the curvature offset to finalize the application of Snell’s law. Finally, we revert the coordinate system back to its original configuration.

B. Deep optics pipeline

In this section, we present more implementation details for deep optics pipeline in both training and testing.

B.1. Rendering by PSF map

Rather than rendering the imaging result pixel by pixel, we first generate the Point Spread Function (PSF) Map through ray tracing. Once the PSF Map is obtained, we compute the camera imaging result using spatially-variant convolution between the PSF Map and the sharp image, illustrated by Fig. A1.

In this paper, we adopt the differentiable PSF map method from [42]. In our experiments, we utilize 51×51 PSF kernel size and 8×8 PSF grid map.

B.2. Tolerance optimization and evaluation

Tolerance optimization. During the tolerance optimization process, we need to simultaneously sample various tolerance modes and perform ray tracing. To mitigate computational overhead, we conduct local ray tracing within a distinct field of view for each sampled tolerance mode, allowing us to obtain the PSF at specific local field of view angles. In our experiments, we sample 64 tolerance patterns, rendering a local PSF for each pattern. Finally, we combine all 64 local PSFs into an integrated PSF map that encapsulates the effects of all tolerance patterns, demonstrated in Fig. A2. It is important to note that we utilize resized images (256×256) from the DIV2K dataset [1] during the training process to mitigate memory overhead, batch size is

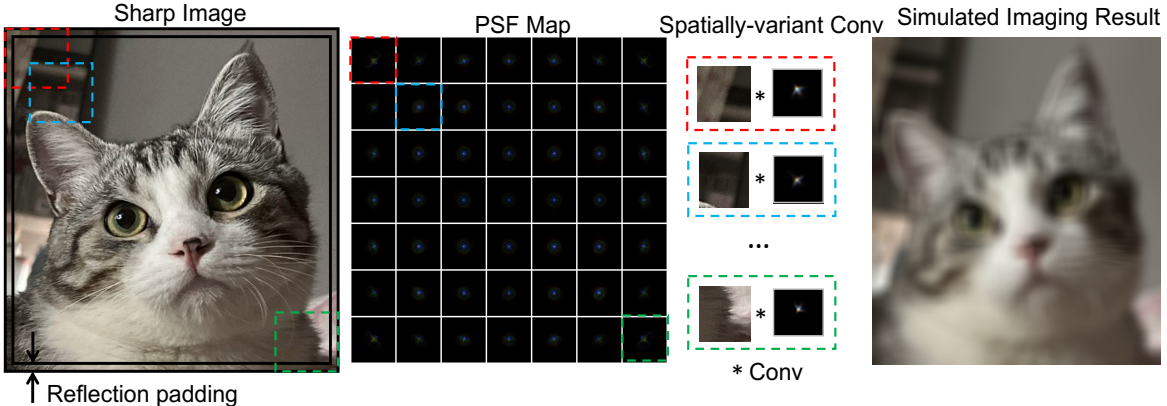


Figure A1. Initially, the original image is populated with reflections. Subsequently, images at various field-of-view positions within the complete large image are convolved using the point spread function (PSF) corresponding to each field-of-view as the convolution kernel. Finally, the convolved images are integrated to produce a cohesive composite.

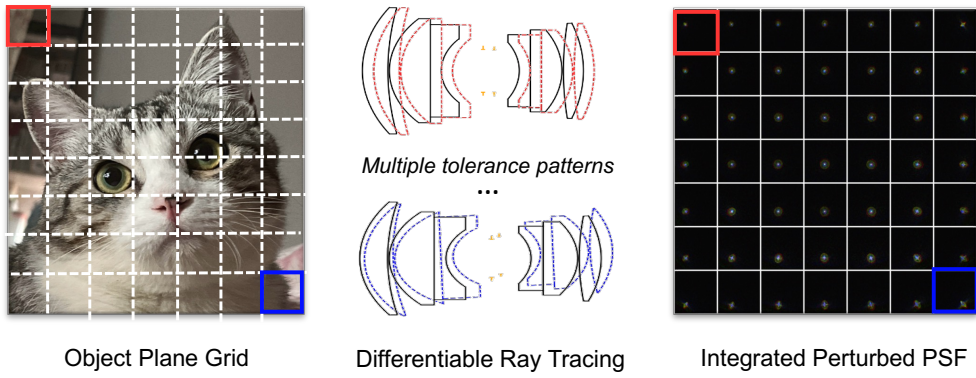


Figure A2. For each local field of view (FoV), a random tolerance pattern is sampled, and the local Point Spread Function (PSF) is obtained through differentiable ray tracing. These local PSFs are then stitched together to create a PSF map that incorporates multiple tolerance patterns.

set in 64. During tolerance optimization, we employ each localized PSF from the PSF map alongside a 256×256 image for convolution to obtain simulated imaging results. Finally, we add 1% Gaussian noise to simulate sensor noise, as shown in Fig. 3.

Evaluation. During evaluation, in contrast to the training phase, we directly utilize 2048×2048 images along with a PSF map obtained from ray tracing, applying spatially-variant convolution to generate simulated imaging results, batch size is set in 2. We sampled randomized tolerances multiple times, and for each sampled tolerance pattern, we computed the PSNR, SSIM and LPIPS, across the entire test dataset.

We visualize the frequency histograms of the complete test results for Lens 1 and Lens 2, see Fig. A3. We provide a visual flipping comparison in the local web page, please refer to the file *visualization.html* in the supplement.

C. Lens1 and Lens2 parameters

In this section, we list all parameters of lens1 and lens2 in Tab. A2 and Tab. A3, and the layouts for the two lenses are as shown in Fig. A4 and Fig. A5.

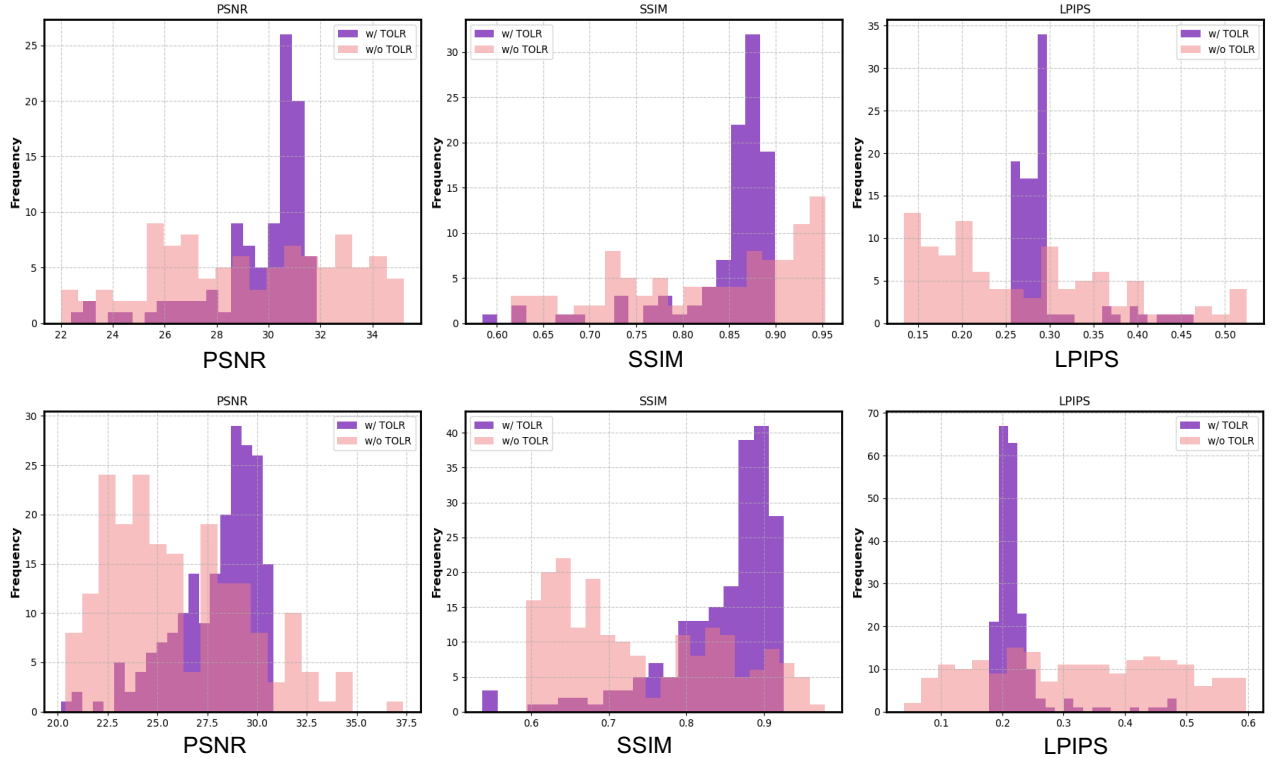


Figure A3. Top: 100 times of random tolerances test for Lens1. Bottom: 200 times of random tolerances test for Lens2. The frequency distribution of the overall test indicates that the deep optics design, following tolerance-aware optimization, is significantly less impacted by tolerances.

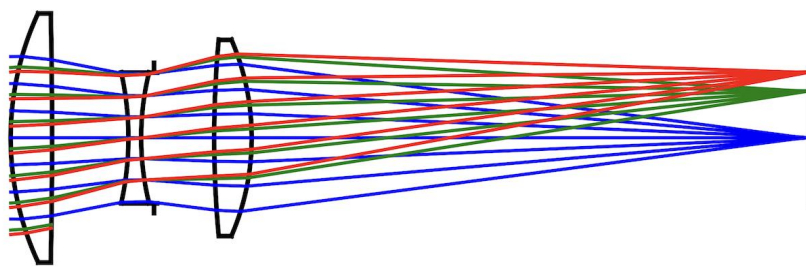


Figure A4. Lens1 layout.

Table A2. The lens1 parameters used in our paper.

Surface No.	Radius (mm)	Distance (mm)	Diameter (mm)	n_d	ν_d
OBJ	INFINITY	1000.0	INFINITY	AIR	
1	22.01	3.26	19.0	1.620410	60.323649
2	-435.76	6.01	19.0	AIR	
3	-22.21	1.0	10.0	1.620040	36.376491
4	20.29	1.0	10.0	AIR	
STO	INFINITY	4.75	10.0	AIR	
5	79.68	2.95	15.0	1.620410	60.323649
6	-18.40	41.55	15.0	AIR	
IMA	INFINITY	-	10.14	AIR	

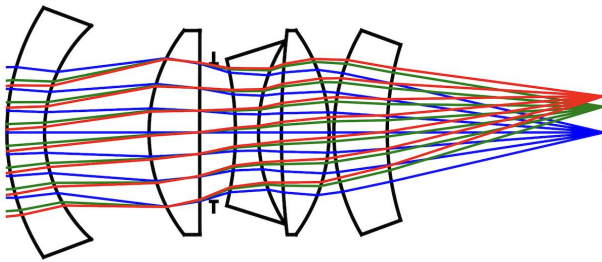


Figure A5. Lens2 layout.

Table A3. The lens2 parameters used in our paper.

Surface No.	Radius (mm)	Distance (mm)	Diameter (mm)	n_d	ν_d
OBJ	INFINITY	2000.0	INFINITY	AIR	
1	37.789	6.544	42.0	1.6400	60.20
2	23.941	18.170	35.984	AIR	
3	27.340	8.800	34.400	1.7880	47.49
4	2541.820	2.432	34.400	AIR	
STO	INFINITY	3.800	23.200	AIR	
5	-50.594	4.000	24.640	1.7552	27.53
6	28.004	3.994	30.862	AIR	
7	149.795	8.285	34.400	1.6400	60.20
8	-28.474	0.832	34.400	AIR	
9	33.206	9.275	34.400	1.6584	50.85
10	47.804	35.074	29.560	AIR	
IMA	INFINITY	-	12.454	AIR	